Research Article

Muhammad Firdaus Abdul Halim, Mohd Sapuan Salit*, Vasi Uddin Siddiqui, Atiqah Mohd Afdzaluddin and Edi Syams Zainudin

Piezoelectric and electrical properties of arrowroot nanocrystalline cellulose-reinforced starch biopolymer composite films for piezoelectric applications

https://doi.org/10.1515/ntrev-2025-0299
Received January 5, 2026; accepted March 18, 2026;
published online May 26, 2026

Abstract: This study investigates the use of arrowroot nanocrystalline cellulose (ANCC) which is a bio-derived nano-reinforcement in the creation of advanced arrowroot starch (AS) biopolymer nanocomposite films. The results demonstrate that ANCC enables tunable piezoelectric and electrical functionality. The incorporation of ANCC into an AS matrix elevates its piezoelectric response, with the longitudinal piezoelectric coefficient (d_{33}) increases from a negligible 2.5 pC/N in pristine AS to 27.3 pC/N at an optimal 3 % ANCC loading with an approximately tenfold increase was observed corroborated by nanoscale piezoresponse force microscopy (PFM) imaging. Concurrently, these nanocomposites exhibit an increase in electrical conductivity and also decreasing resistivity from a highly insulating $19{,}600 \times 10^{-3}\,\Omega\,\text{mm}$ to higher conductive $3{,}806 \times 10^{-3}\,\Omega\,\text{mm}$ with 10 % ANCC. It was discovered that the film resistivity dropped drastically as ANCC concentration increased. Highest at $19{,}600 \times 10^{-3}\,\Omega\,\text{mm}$ was achieved in the control sample, whereas the lowest $3{,}806 \times 10^{-3}\,\Omega\,\text{mm}$ was the AS/ANCC10. This shows that ANCC significantly enhances the electrical responsiveness of the starch matrix and indicate potential for application in sustainable, high-performance components of sensing, actuation, and flexible electronics.

***Corresponding author: Mohd Sapuan Salit**, Advanced Engineering Materials and Composites Research Centre (AEMC), Mechanical and Manufacturing Engineering, Universiti Putra Malaysia, 43400 UPM, Serdang, Selangor, Malaysia, E-mail: sapuan@upm.edu.my
Muhammad Firdaus Abdul Halim, Vasi Uddin Siddiqui and Edi Syams Zainudin, Advanced Engineering Materials and Composites Research Centre (AEMC), Mechanical and Manufacturing Engineering, Universiti Putra Malaysia, 43400 UPM, Serdang, Selangor, Malaysia
Atiqah Mohd Afdzaluddin, Institute of Microengineering and Nanoelectronics (IMEN), Universiti Kebangsaan Malaysia (UKM), Bangi, Selangor, Malaysia

Keywords: piezoelectric; electrical; nanocrystalline cellulose

1 Introduction

Piezoelectricity represents a fascinating phenomenon according to which a set of materials exhibit the capacity to produce an electric charge when a mechanical stress is involved in them, and vice versa, to experience a mechanical deformation when an electric field is applied to them [1]. This unique electromechanical interaction is what renders piezoelectric materials of significant value across a vast variety of applications, both in everyday consumer electronics, as well as in high-end medical and industrial equipment and sensors [2]. The term “piezo” itself derives its name in the greek word “piezein”, which means to squeeze or press and is befitting in relation to the mechanical-electrical interaction [3]. Piezoelectricity was also found in quartz, a naturally occurring crystal, the discovery by Pierre and Jacques Curie in 1880 [4]. PZT ceramics are extensively used synthetic piezoelectric materials that have a strong piezoelectric response and that also exhibit tunable behavior [5].

The principle that forms the basis of piezoelectricity is based on the crystallographic principle of the material. The unit cells of piezoelectric materials are not centered in their respective cells [6]. Upon the application of mechanical stress, the atoms that make up these non-centrosymmetric lattices move thus causing the locations of positive and negative charge to be displaced [7]. Such segregation of charge creates an electric dipole moment which produces a detectable voltage between the surfaces all around the material. On the other hand the employment of an external electric field positions the dipoles in the field leading to the deformation of the material and the subsequent change in shape; the opposite effect, the converse piezoelectric effect, is called [8].

One of the properties that enable the calculation of the ability of a material to conduct electric current is electrical

conductivity [9]. It is the converse of electrical resistivity that measures the resistance presented by a material to current flow [9]. The principle of electrical conductivity is inherently intuited with the movement of charge carriers, or electrons or ions, in a material due to the influence of an electric field [10]. One generally categorizes materials by their capacitance: conductors (e.g., metals) have high capacitance, allowing free flow of current; insulators (e.g., rubber or glass) have very low capacitance, and effectively resist current passage; and semiconductors (e.g., silicon) have middle capacitance that can be easily adjusted [10].

Nanocellulose or graphene reinforced biopolymer composites, created based on renewable natural polymers (starch or cellulose), have become particularly popular compared to traditional petroleum-based polymers due to their improved environmental sustainability, biodegradability, and reduced carbon footprint [11]. Unlike synthetic polymers like polyethylene or polypropylene, which rely on the non-renewable fossil reserves and contribute significantly to plastic pollution, biopolymer composites are an environmentally friendly material, which offers better mechanical, thermal and barrier properties by means of nanoreinforcing [12]. Experimental studies of such materials are central, as they enhance the understanding of the interfacial contact between natural polymer matrix and nanofillers, and, thus, they enable the development of sustainable and high performance materials that can be applied to various purposes not only in packaging, but also in biomedical devices and flexible electronics, and, ultimately, support the transition to green and circular material systems in the world [13].

Incorporation of a bio-based filler, that is, arrowroot nanocrystalline cellulose (ANCC) into a starch biopolymer matrix is a sustainable and environmentally benign replacement of the conventional ceramic fillers in piezoelectric processes [14]. Unlike ceramics like barium titanate or zinc oxide which are brittle, non-biodegradable, and need to undergo a high-temperature procedure, ANCC exhibits a high level of compatibility with the starch matrix through strong formation of hydrogen bonds, therefore, enhancing mechanical flexibility, homogenous dispersion, and effective transfer of stress in the composite [15]. This bio-based reinforcement maintains the biodegradability and at the same time increases the dielectric and piezoelectric properties that makes this material fit the requirements of flexible and wearable applications, such as pressure sensors, energy harvesters, and biomedical sensors. Therefore, the integration of ANCC helps to make lightweight piezoelectric films biocompatible and affordable, thus promoting green and sustainable electronic technologies.

The main distinction between arrowroot nanocrystalline cellulose (ANCC) and cellulose made of wood, bamboo, or sisal is high purity, low lignin content, and smaller crystal size, which produce easy extraction and enhance dispersion in polymer matrices [16]. These properties increase the interfacial bonding and compatibility with the starch when compared to cellulose that is obtained through the lignocellulosic sources, which normally undergoes intensive chemical treatments. Meanwhile, arrowroot starch has a better performance in comparison to cassava and corn starch, such as, it has a higher amylose concentration, smaller granule size, better film-forming capacity, and higher thermal and mechanical stability [14]. Arrowroot starch and ANCC have been combined to form a highly compatible, sustainable and entirely bio-based composite system with high flexibilities, transparency and performance in packaging and piezoelectric applications.

Arrowroot starch (AS) is a natural, biodegradable polysaccharide extracted from the tubers of widely used in food and biopolymer applications due to its excellent film-forming and thickening properties [17]. Nanocrystalline cellulose is a type of nanocellulose, which are naturally occurring cellulose fibers that have been broken down into their nanoscale crystalline components [18]. These nanoparticles possess unique and highly desirable properties due to their high crystallinity, high aspect ratio (length to width), high strength, stiffness, and large surface area [19]. Figure 1 shows the arrowroot plant and arrowroot tuber.

Recent research indicates that the electrical conductivity of biopolymer nanocomposites is influenced by numerous factors, including the distribution, shape, size, and aspect ratio of fillers, filler conductivity, interactions with the polymer matrix, matrix nature, wettability, orientation, surface energy, and processing techniques. Based on these complex factors, various models have been developed

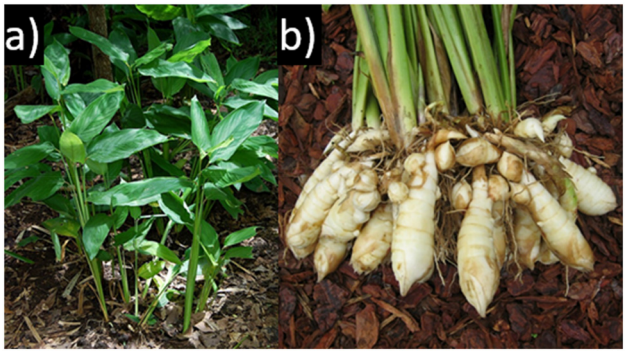

Figure 1: (a) Arrowroot plant, (b) arrowroot tuber.

to predict the electrical conductivity, resistivity, and piezoelectricity of these materials [20].

Considering the complex nature of the factors influencing these properties, it is such an important need to have a better grasp of the relationship between the theoretical approximations based on the theoretical models presented and the experimental values taken to be the actual in the specific areas of electrical conductivity, resistivity, and piezoelectricity. The existing use of the volume fraction solely has been frequently inadequate to realistically gain insight into the complex interactions of all the contributing parameters and results in variances between the theoretical extrapolations and actual performance. The prerequisite to functional biopolymer nanocomposites is the urgent need to bridge this gap in knowledge in order to develop and optimize the nanocomposites for specific uses. In line with this, this manuscript meets this requirement by clearly discussing each AS/ANCC sample that has been used by scholars in predicting the electrical and piezoelectric characteristics of the AS/ANCC system. The paper addresses the aim of improving the predictive characterisation of biopolymer nanocomposites through a critical study of these models.

2 Experimental

2.1 Materials

The Arrowroot tuber (*Maranta arundinacea*) was obtained at Norient Jaya Sdn. Bhd, Kuala Lumpur, Malaysia. The tubers were exposed to a rigorous washing regimen which was meant to remove various dirts and impurities on the surface and consequently, the tubers were peeled and sliced and dried at 50 °C after which they were ground into a fine powder. The bagasse fiber of arrowroot used in this research contains cellulose 45.97 %, hemicellulose 30.18 %, lignin 2.78 %, ash 4.29 %, and fiber sizes (<300 μm) [21]. The resulting arrowroot fibre was then sieved to achieve particles whose diameter was below 300 μm. The acid hydrolysate was then converted into arrowroot nanocrystalline cellulose (ANCC) using 55 % of H_2SO_4 based on the procedure described by Ilyas et al. [22]. Hydrolysed suspension was centrifuged, washed until it attained a neutral pH, dialysed and freeze-dried to produce ANCC powder.

The extraction of arrowroot starch (AS) was done in fresh tubers according to the protocol by Tarique et al. [21]. The process was done by mixing the tubers with distilled water, after which they were filtered, sedimented, and dried at 50 °C before being ground into a fine starch powder. The glycerol and sorbitol used as plasticisers in the method of making the composite film were obtained in Evergreen Engineering and Resources Sdn. Bhd., Selangor, Malaysia.

2.2 Film preparation

Nanocomposite films of biopolymers were prepared at advanced engineering materials and composites (AEMC) Lab of Universiti Putra Malaysia using the solution casting method. ANCC aqueous suspension was prepared with different concentrations (1–10 wt%) with respect to arrowroot starch (AS). The formation of the film was accomplished by dissolving 10 g of AS in 180 mL of distilled water with vigorous stirring. To improve the flexibility and reduce the brittleness, a plasticizer of glycerol and sorbitol (1:1) solution of 30 % was added. The mixture of 1:1 glycerol/sorbitol improves the alignment of the dipoles by increasing flexibilities of the polymer chain with maintaining structural stability. Glycerol augments the chain mobility that promotes the formation of the dipole reorientation during the mechanical stress, and sorbitol provides the modulated plasticisation together with mechanical support. Owning to this balanced plasticisation, more efficient stress transfer and dipole alignment becomes possible, which leads to better piezoelectric performance [23]. It was stirred at 80 °C to attain complete gelatinisation and homogeneous dispersion within 15 min and stirred until it reached ambient temperature.

The 50 g portions of the film-forming solution were then deposited in 13 cm Petri dishes and dried in the oven at 40 °C over a period of 24 h thus giving a homogeneous film as suggested by Prayoon et al. [24]. ANCCs in the form of control film (0 % ANCC) and nanocomposite films with 1 wt%, 3 wt%, 5 wt%, and 10 wt% ANCC were labeled as AS/ANCC1, AS/ANCC3, AS/ANCC5 and AS/ANCC10. All the films were dried and allowed to equilibrate at 25 °C in a period of 24 h after the process of drying and then kept at 25 ± 3 °C and 52 % relative humidity in a week before characterization. At higher humidity, starch-based films absorb more moisture, which increases polymer chain mobility and ionic conduction, potentially disrupting dipole alignment, reducing the piezoelectric coefficient (d_{33}), and lowering electrical stability due to leakage effects and softening of the material. On the other hand, dryness makes the films drier and less compliant, which has been found to increase the stability of the dipole and also it makes the materials brittle, but overly dry can lead to brittle materials [25]. Therefore, humidity significantly influences the electromechanical performance and stability of starch-based composites. Figure 2 illustrates the flow of the fabrication process, and Table 1 presents the formulae of composition of the AS/ANCC biopolymer nanocomposite films in table.

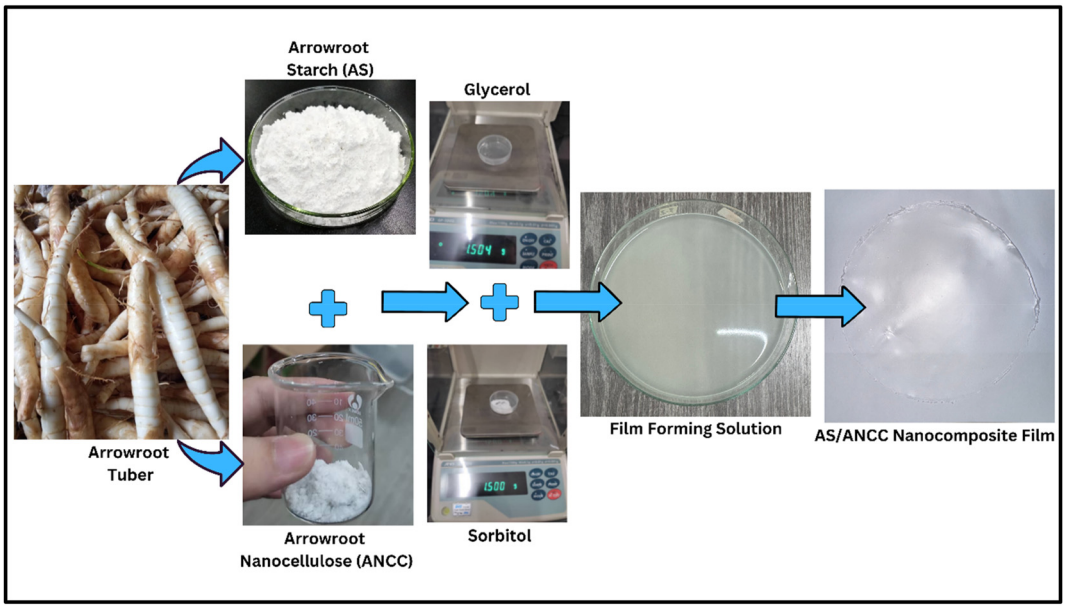

Figure 2: The biopolymer film preparation process.

Table 1: A composite formulation for AS/ANCC biopolymer nanocomposite film.

Composite	Starch (g)	Nanocellulose loading (%)	Glycerol (g)	Sorbitol (g)	Distilled water (mL)
Control	10	0	1.5	1.5	180
ANCC/AS1	10	1	1.5	1.5	180
ANCC/AS3	10	3	1.5	1.5	180
ANCC/AS5	10	5	1.5	1.5	180
ANCC/AS10	10	10	1.5	1.5	180

2.3 Characterization

2.3.1 Piezoelectric properties

2.3.1.1 Piezoelectric coefficient, d_{33}

Piezoelectric performance was evaluated by measuring the longitudinal piezoelectric coefficient (d_{33}) with a YE2730A d_{33} meter (APC International, Ltd., USA) as shown in Figure 3. The sample was cut into 2×2 cm pieces, with three replicates prepared for each sample. The meter sensitivity covering a range of 1–200 pC/N, allowed for a direct comparison of the obtained d_{33} values against established literature.

Figure 3: YE2730A piezoelectric coefficient, d_{33} meter.

2.3.1.2 Piezoresponse force microscopy (PFM)

The local nanoscale piezoelectric response of all film samples was analyzed using PFM. This involved scanning 10 different 1 μm^2 areas on each film's surface. A MULTI75-EG cantilever was employed for these measurements. An alternating current (AC) driving amplitude (V_{AC}) ranging from 1 to 5 V was applied to the tip at a frequency of 3 kHz. This frequency was chosen to be well below the cantilever's contact resonance, thus preventing signal interference (crosstalk) between the simultaneously recorded topography and piezoelectric response. The piezoelectric response along the *z*-direction was quantified as the first

harmonic of the bias-induced tip deflection (d), consistent with the method described by Signore et al. [26]:

$$d = d_o + A\cos(\omega t + \varphi) \quad (1)$$

where d_0 represents the equilibrium position of the tip, A is the amplitude, and ω denotes the frequency of the applied bias. The phase, φ, provides information about the polarization direction beneath the tip. Both amplitude and phase signals from PFM were collected to analyze the piezoelectric characteristics of the samples under investigation.

2.3.2 Electrical properties

The film was fabricated according to the required dimensions for compatibility with the four-probe test apparatus. Keithly 2,400 source metre SMU instruments (Tektronix, Beaverton, or, United States) in DC mode and a four-point probe MST-2000A four-point probe system (MSTECH Co., Ltd., South Korea) were used for the measurement of current–voltage (I–V), as illustrated in Figure 4. To determine the electrical resistivity and conductivity of the AS/ANCC biopolymer nanocomposite films, the four-probe method was employed, as presented in Figure 5. This method, conducted under constant temperature conditions, was used to measure the resistance (R) of the samples. The electrical conductivity (σ) was calculated as the reciprocal of the resistivity (ρ), considering the effective length (L) between the outer probes. The spacing (S) between each adjacent probe was fixed at 1 mm.

$$\text{Ohm}'\text{s Law V} = \text{IR} \quad (2)$$

where: V = voltage, I = current.

$$\text{Resistivity } \rho = 2\pi SR\ [\Omega \quad \text{m}] \quad (3)$$

$$\text{Conductivity } \sigma = 1/\rho\ [\text{S/m}] \quad (4)$$

Based on the equation above, resistivity (ρ) was obtained from the resistance (R) values measured using the four-probe setup. During the measurements, the current was supplied and recorded using a Keithley 236 source measure unit, while the voltage was measured using a Picotest M3500A digital multimeter. In this experiment, the current was kept constant at 0.1 μA, and the corresponding voltage was recorded for each sample. The resistance was then calculated using ohm's law, as shown in eq. (2).

The resistivity (ρ) is expressed in ohm milimeters (Ω mm), which is the standard unit for measuring the intrinsic resistance of a material. Semiconductors are materials that exhibit electrical conductivity values between those of conductors and insulators. As shown in eq. (3), the electrical conductivity (σ) is inversely proportional to resistivity and is expressed in siemens per meter (S/m).

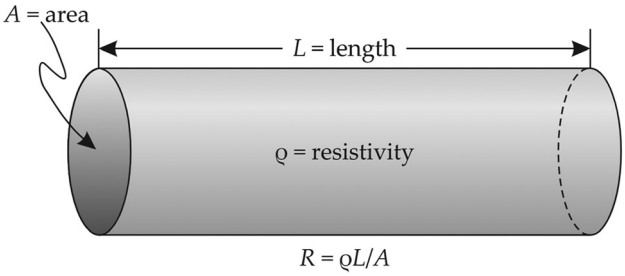

Figure 5: Electrical conductor [28].

3 Results and discussions

3.1 Piezoelectric coefficient, d_{33}

Table 2 compares d_{33} in the various composite materials. The comparison of diverse composite materials draws a wide range of their piezoelectric coefficients (d_{33}), which indicate their different abilities as piezoelectric materials. The conventional ceramics such as BaTiO3 and PZT has relatively high value where BaTiO3 has a maximum value of 416 pC/N

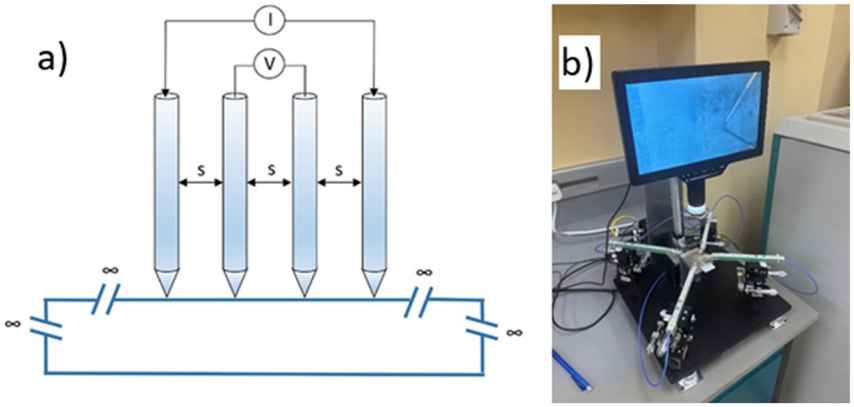

Figure 4: (a) The visualization of four probes, (b) the setup of four probes to the surface of the biopolymer nanocomposite film [27].

(picocoulombs per Newton) in the presence of nanomaterials. The values of d_{33} are also very high in lead-based ceramics such as in $PbTiO_3$ to 350 pC/N indicating great piezoelectric behaviors. PVDF and copolymers exhibit lower d_{33} with 17–33 pC/N, and higher-order polymers such as microporous PTFE/PFCB polymers exhibit higher d_{33} of up to 600 pC/N. Intermediate performance has been shown by organic and inorganic hybrids such as $TMCM_2SnCl_6$ and metal-doped ZnO. And particularly, potassium sodium niobate (KNN) ceramics represent a lead-free, and they are remarkable in terms of transport crystal structure, having a d_{33} values of 208.2 pC/N to 330.7 pC/N, which highlights their possibility to be implemented into sustainable piezoelectric applications.

Figure 6 illustrates a bar chart displays the d_{33} in pC/N for AS composites with varying concentrations of ANCC. A d_{33} coefficient is an important value that is used to assess piezoelectric response of a material and this measures the amount of electric charge that is produced with the change in mechanical force or the other way round [43]. An evaluation of such data indicates that there is a definite correlation on ANNC concentration and piezoelectric performance of the composite. The plasticizers deliberately included glycerol and sorbitol to bring about plastics and curb brittle. Though can have some influence on the dielectric constant and charge mobility, they ease the piezoelectric and levels transfer in the matrix hence bearing positive impact on the piezoelectric and electrical responses.

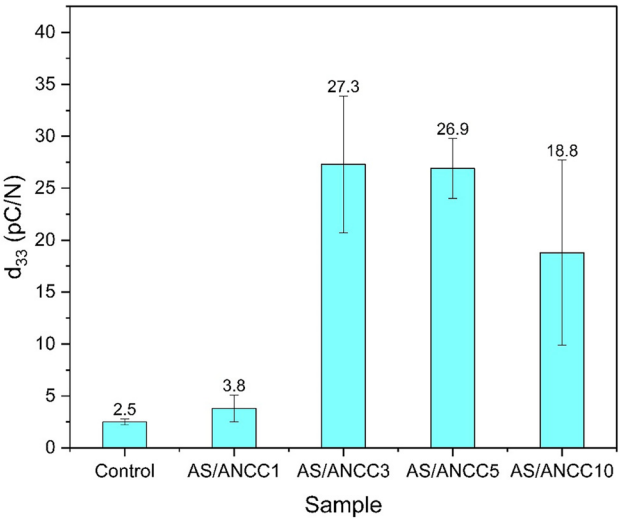

Figure 6: Piezoelectric coefficient (d_{33}) of AS/ANCC biopolymer nanocomposite films.

The control sample as a pure AS with 0 % ANCC has the very low d_{33} of about 2.5 pC/N. It means that AS itself is hardly intrinsically piezoelectric [44]. Addition of a low concentration of ANCC, 1 % in the AS/ANCC1 sample results in the slight rise of the d_{33} value to approximately 3.8 pC/N. Though this is a little higher than control sample did not prove significant enhancement at this low ANCC concentration of piezoelectric properties [45].

AS/ANCC3 sample indicates that there is a very high increase in piezoelectricity at the ANCC concentration of 3 %

Table 2: Comparison of d_{33} in different composites materials.

Authors	Composite materials	Piezoelectric coefficient, d_{33} (pC/N)
Xu et al. [29]	Lysozyme films	0.94–3.16
Kim et al. [30]	Di-phenylalanine (FF)	18 ± 5
Kim et al. [30]	Poly-γ-benzyl-L-glutamate (PBLG) synthetic polypeptides	25
Kim et al. [30]	Poly(-benzyl-L-glutamate)/Poly(methyl methacrylate) PBLG-PMMA	23
Shua et al. [31]	Lead titanate, $PbTiO_3$ nanoparticles	95–240
Huang et al. [32]	Trimethylchloromethylammonium tin hexachloride ($TMCM_2SnCl_6$)	137
Gasperini et al. [33]	Ceramic lead zirconate titanate (PZT) nanofibers	39
Zong-Yang Shen et al. [34]	Barium titanate $BaTiO_3$ ceramics	190
Zong-Yang Shen et al. [34]	Barium titanate $BaTiO_3$ with nanomaterials	416
Yang et al. [35]	Flexible poly(vinylidene fluoride) (PVDF)	17–33
Ge et al. [36]	Potassium niobate, KNbO3 nanocubes	105
Achidi Frick et al. [37]	Poly(vinylidene fluoride) Trifluoroethylene (PVDF-TrFE) used.	20.3
Lee et al. [38]	Potassium sodium niobate, $(K,Na)NbO_3$ ceramics	208.2–330.7
Kirkpatrick et al. [39]	3D printed polyvinylidene fluoride (PVDF).	0.36
Neugschwandtner et al. [40]	Microporous polytetrafluoroethylene, PTFE and perfluorinated cyclobutene, PFCB polymer layers	600
Yang et al. [41]	Vanadium reinforced zinc oxide	110
Acharya et al. [42]	Lanthanum reinforced lead barium niobate ceramics.	350

of the total composition. When this value (d_{33}) increases to some 27.3 pC/N, this is a significant increase in compared to the control and the 1 % ANCC samples. It means that ANNC 3 % is very efficient to improve the piezoelectric characteristics of composite. The latter might be maintained by such strong performance found in the AS/ANCC5 sample, where the d_{33} is approximately 26.9 pC/N which is quite close to the 3 % concentration. These experiments indicate that the ANNC range of 3–5 % gives the greatest maximization of the piezoelectric response.

However, with a further addition of the ANCC concentration to 10 % in the AS/ANCC10 sample, the value of d_{33} reduces significantly to approximately 18.8 pC/N. Although the AS/ANCC10 sample also presents an improvement equally to the control and AS/ANCC1 samples, its d_{33} value is low as compared to the optimum that is realized at 3 % and 5 % ANCC loading. This decrease at higher concentrations could be explained by aggregation or agglomeration of ANCC nanoparticles that could inhibit the efficiency of dispersion and the individual contribution of each of the components to the overall piezoelectric activity [46]. Therefore, the data of d_{33} show that addition of ANCC enhances piezoelectric performance of AS significantly, and the most efficient level of inclusion concentration is between 3 % and 5 %.

Even though the gain in d_{33} with 2.5 pC/N to 27.3 pC/N is a significant improvement to a fully bio-based system, it is by far lower than the usual ceramic piezoelectric materials, including PZT (±350 pC/N) and $BaTiO_3$ (±416 pC/N) [47]. This performance gap is expected due to the intrinsic ferroelectric crystal symmetry present in ceramics, which is absent in polymer-based systems, which possess highly ordered non-centrosymmetric crystal structures that enable strong polarization. However, the objective of AS/ANCC composites is not to directly compete with high-voltage ceramic actuators, but rather to offer a sustainable, lightweight, flexible, biodegradable, and low-cost alternative for low-power sensing and wearable applications. While ceramics deliver high piezoelectric output, they suffer from brittleness, toxicity (lead content in PZT), high processing temperatures, and lack of biodegradability. Therefore, the trade-off between sustainability and peak voltage output must be considered application-specific, where moderate piezoelectric response combined with environmental compatibility and mechanical flexibility may be more advantageous for next-generation green electronics.

The presence of agglomeration in the specimens reduces piezoelectric behavior mainly due to the ineffective transfer of homogeneous stress and poor dipole alignment caused by ANCC clustering within the composite matrix [48]. In a well-dispersed system, individual nanocrystals are uniformly distributed throughout the starch backbone, providing a maximum interfacial area and enabling efficient mechanical-to-electrical energy conversion through cooperative dipole orientation. In contrast, agglomeration leads to the formation of localized clusters that reduce effective surface interaction with the matrix [49]. Such clusters become a mechanical defect and high concentration of strain leading to the non-uniform distribution of strain under the exerted force. As a result, less efficient polarization contributes to the polarization due to less polarization of such a smaller number of dipoles and decreases the overall d_{33} response. Also, agglomerated regions can bedevil the movement of the polymer chains and interfacial polarization and at the same time they provide internal polarization charge traps between polymer strands that diminish the electrical signal detected. Hence, there is net decreasing net piezoelectric performance even though filler loading is increased and finally, poor dispersion prevents pitting and further leads to poor net piezoelectric performance.

3.2 Piezoresponse force microscopy (PFM)

Figure 7 indicates that the apparent trend obtained through the analysis of the analyses of the PFM amplitude, which is indicative of the piezoelectric response, tends to get larger and more pronounced with higher concentrations of nanomaterials [50] and it appears to reach its highest point and possibly ends up equalizing and even reducing with further higher concentrations. Among amplitude mapping, phase (ϕ) images were also recorded when analyzing PFM. Oppositely oriented polarization domains were seen in the ANCC-reinforced samples by a distinct phase contrast of (~180°) and the existence of non-centrosymmetric dipole structures in the composite films were affirmed.

The control sample, as the sample with 0 % ANCC, has an exceptionally low amplitude of the PFM, mostly with the range 0–50 mV without any differentiated or regular waveform that can be identified [51]. This indicates that pure AS has a low or zero intrinsic piezoelectricity when it is measured in the specified conditions [52]. The level of ANCC introduced, as with the AS/ANCC1 sample (1 % of ANCC), causes a minor modification. The PFM amplitude does not vary much, as although the values change somewhat, it is still mostly less than 100 mV, and this concentration is not enough to noticeably cause or lead to an effective piezoelectric response [53].

Nonetheless, there is a great modification in the case of the AS/ANCC3 sample, which contains 3 % ANCC. In this case, the amplitude of PFM is significantly high, and the signal has a definite periodic and wave-like fractal [54]. Peak amplitudes always lie within the range of 250 mV–450 mV which

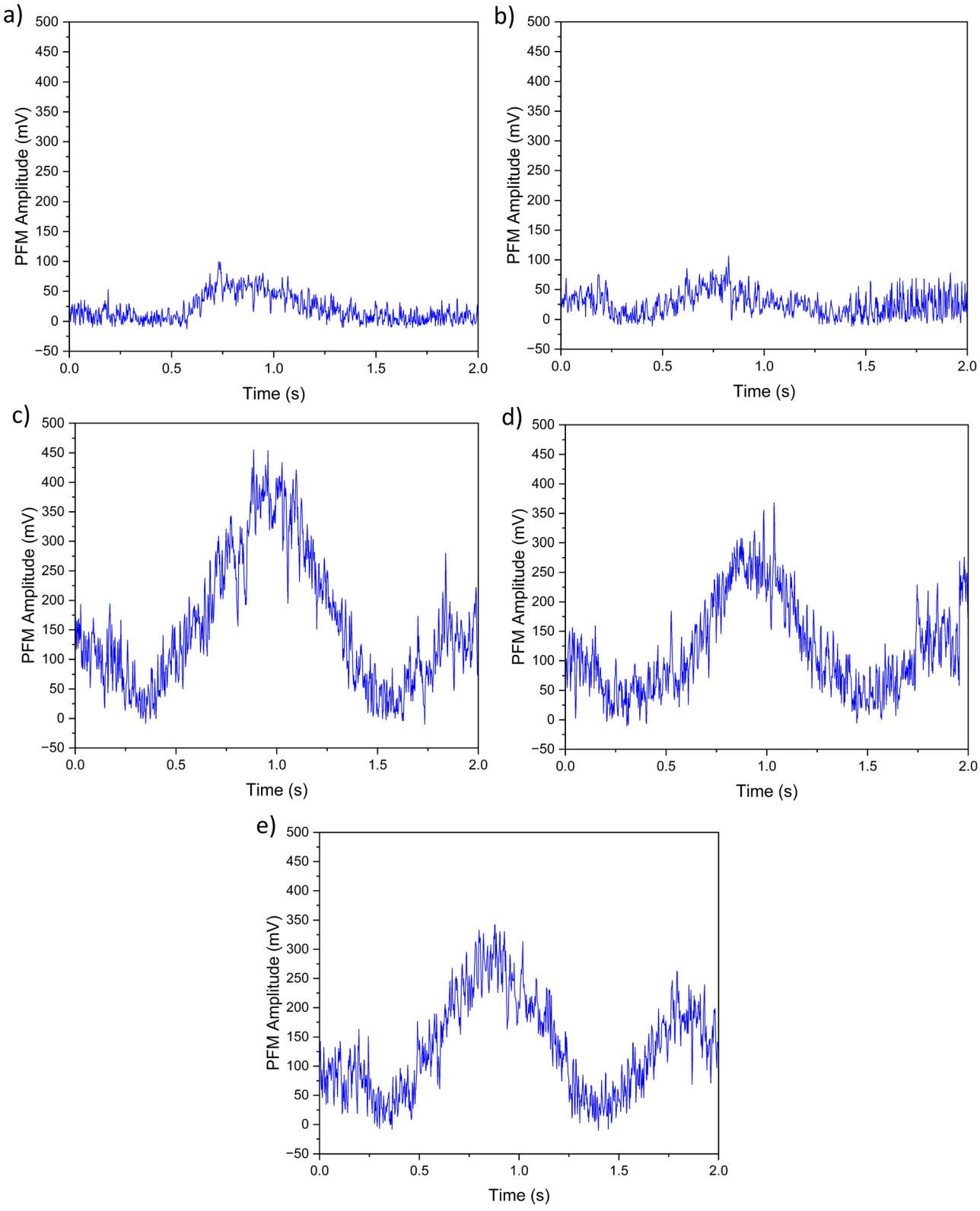

Figure 7: Piezo-response force microscopy (PFM) of AS/ANCC biopolymer nanocomposite films; a) control film sample, b) AS/ANCC1 film sample, c) AS/ANCC3 film sample, AS/ANCC5 film sample and AS/ANCC10 film sample.

proves to be considerably higher and more pronounced piezoelectric response than the control and 1 % ANCC samples. This implies that 3 % ANCC is successful in improving the piezoelectric performance of the composite [55]. This increased response is continued and seems strong in the AS/ANCC5 sample (5 % ANCC) where the PFM amplitude is high, and the amplitude of the peaks is consistently in between 250 mV and 400 mV that it behaves substantially piezoelectric.

At the optimal concentration, AS/ANCC10 (10 % ANCC) the PFM amplitude is significant with its obvious periodicity that is also comparable with the 3 % and 5 % ANCC samples. Nevertheless, the amplitudes of the peaks, which are normally between 250 and 350 mV, would seem not to significantly surpass those at 3 % patterns and 5 % patterns of ANCC, and in certain cases, would be a little smaller. To sum up, this research points out that the addition of ANCC can greatly improve the piezoelectricity of AS with a preferable concentration apparently obtained in the regions of 3 %–5 %.

3.3 Measurement of voltage (*V*) with current (pA)

Figure 8 shows that the current-voltage (I-V) properties of nanocomposite films of AS biopolymer as a function of ANCC concentration. These curves are important in explaining the electrical behavior of such materials especially their conduct ones and non-ohmic behavior. The first observation is that there is non-linear diode-like behaviour in all the samples which means that the resistance to electrical conduction does depend on the applied current or voltage as in simple ohmic materials. Control sample (0 % ANCC) has the greatest resistance, which is indicated with a relatively slow rise in current with a rise in voltage, particularly at lower currents.

Introducing ANCC provokes a certain change towards increased conductivity. The sample of AS/ANCC3, AS/ANCC5, and especially AS/ANCC10 exhibit higher frequency of voltage to current-voltage ratio increment. The sample, which has the greatest ANCC concentration (AS/ANCC10), has the steepest slope on the first region of its curve which means that it has the least resistance and greatest conductivity at the lower values of these currents. It also achieves a premium current plateau at a faster rate of time as compared to the other samples under the same voltage.

These patterns in these I-V curves are predictable to previously reported data on resistivity and conductivity: growth in ANCC concentration generally results in electrically conductive films. This is supported graphically by the movement of the curves towards an increase in currents at a given lower applied voltage. The non-linear behavior, taken

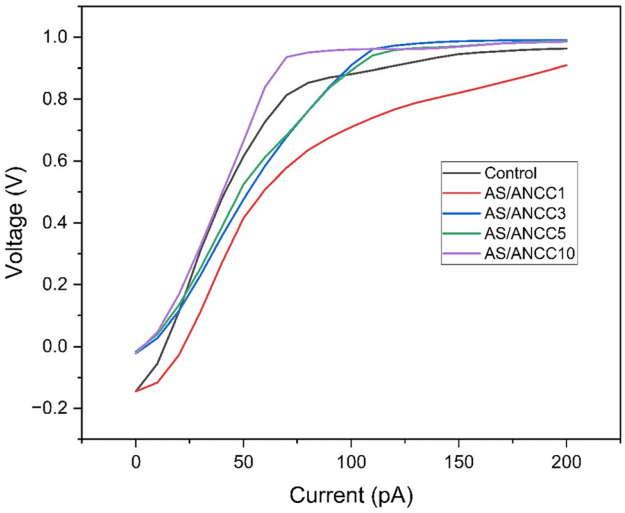

Figure 8: Voltage versus current of AS/ANCC biopolymer nanocomposite films.

consistently among all the samples means that there are complicated processes of charge-transport, which may be compelled by the interfaces between ANCC and the AS matrix [56]. This repetitive trend strongly supports the idea that ANCC is efficient to improve the transport of charge in these composite films.

The AS/ANCC3 and AS/ANCC5 samples have negative steeper slopes and greater voltage response at lower currents as compared to the control and the AS/ANCC1 formulation, indicating that they spread better and resulted in stronger interfacial communications between the two. The nanocrystalline cellulose which has been incorporated is likely to enhance interfacial polarization and charge hopping due to decreasing the distance between particles to form a partial conductive network [57]. The limitation in gained conductivity of further loading though seems to be due to the tendency of agglomeration since the development of charge-trapping area and the decrease of effective conducting paths obstruct the performance in AS/ANCC10 with high loading.

3.4 Electrical resistivity

The implantation of ANCC was found to have significant influence on the resistivity of AS biopolymer nanocomposite films as shown in Figure 9. The degree to which any substance prevents the movement of electric current is measured by resistivity which is expressed as Ω mm at a fixed current of 0.1 μA.

There was a clear trend in the data the further into the ANCC concentration, the more film resistivity reduced. As

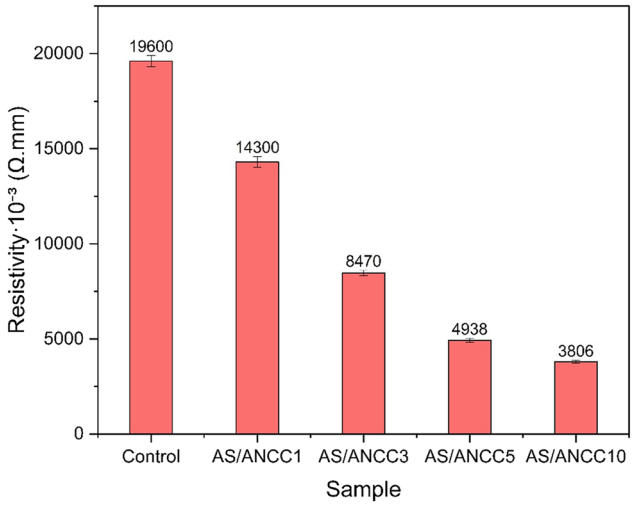

Figure 9: Resistivity of AS/ANCC biopolymer nanocomposite films.

can be seen, the control of pure AS (0 % ANCC) demonstrated the highest resistivity of about 19,600 $\times$ 10^{-3} Ω mm, indicating that the substance is an insulator. Even the slightest increase of 1 % ANCC (AS/ANCC1) led to a drop in the resistivity to approximately 14,300 $\times$ 10^{-3} Ω mm. The resistivity was observed to decrease steadily with further increase of the ANNC concentration: AS/ANCC3 exhibited the maximum resistance of about 8,470 $\times$ 10^{-3} Ω mm; AS/ANCC5 to approximately 4,938 $\times$ 10^{-3} Ω mm; and the AS/ANCC10 to the final value in the series of about 3,806 $\times$ 10^{-3} Ω mm.

The findings show that there is an inverse dependency between the ANCC concentration and electrical resistivity of the AS/ANCC biopolymer nanocomposite films. Accordingly, an increase in the percentage of ANCC results in a decrease in the resistance characteristics of the films [58]. This would imply that ANNC, even though it is of plant nature, is effective in enhancing the electrical conductivity of the AS matrix. This property is especially useful when there is a need of finely tuned electrical properties in applications, such as an insulator to conductive films, and predicts new applications in sustainable technology. A comparative analysis of resistivities was made on different natural or synthetic fiber composite presented in Table 3.

3.5 Electrical conductivity

Figure 10 offers solid arguments that ANCC has a major impact on raising the electric conductivity of AS biopolymer nanocomposite films. The ability of a material to conduct electricity is directly proportional to the product of its electrical conductivity (Siemens per centimeter (S/cm, multiplied by 10^{-6}) in the constant current of 0.1 μA which a good electrical conductor has a higher electrical conductivity number [66].

The statistics make the correlation between the rise in ANCC concentration and better film conductivity evident. The nature of the control sample as a poor electrical conductor was validated by the fact that the sample, which was pure AS (0 % ANCC) saw a rather low conductivity of about 519 $\times$ 10^{-6} S/cm. But conductivity began to increase significantly with addition of ANCC even at low concentration 1 % of ANCC1 to about 699 $\times$ 10^{-6} S/cm. This trend was even greater when there was more ANCC content. Conductivity had risen in the AS/ANCC3 sample to about 1,390 $\times$ 10^{-6} S/cm. This pattern had persisted in the AS/ANCC5 sample, and this led to further increase up to about 2,360 $\times$ 10^{-6} S/cm with further sample. At last, the conductivity was at its highest point at the concentration of 10 0 ANCC (AS/ANCC10) with a result of approximately 2,730 $\times$ 10^{-6} S/cm. Such consistent increasing conductivity augmentation behavior with increasing ANCC content means that ANCC plays a central role of significantly increasing the electrical conductivity of these AS biopolymer nanocomposite films [67].

The findings are positive in a correlation of the electrical conductivity of AS/ANCC biopolymer nanocomposite films against the concentration of ANCC. The more fibers of nanocrystalline cellulose are included into the films, the more the films develop into superior electrical conductors [68]. This highly enhanced conductivity also indicates that ANCC, perhaps because of its natural crystalline character and because of its capability to promote the migration of charge carriers, can be helpful in creating conductive paths in the otherwise insulating AS matrix [69]. These improved electrical capabilities are of enormous benefit to a broad variety of upcoming uses where controlled electrical characteristics of materials, with exceptional fineness, are required, and improve sustainable electronic and sensing technology [70].

4 Conclusion and future prospect

4.1 Conclusions

The present research paper is the report of an essential progress made by the integration of ANCC with AS biopolymer films, which led to a considerable improvement of piezoelectric and electrical properties of films. Pure AS films showed relatively small piezoelectric strength (d_{33} in the range of 2.5 pC/N). This was an increased response on addition of ANCC. Optimum ANCC concentration is 3–5 % formed optimum d_{33} of above 26 pC/N, which demonstrated

Table 3: Comparison of resistivities in different natural/synthetic fiber composites.

Authors	Measurement instrument	Composite materials		Electrical resistivity (Ω mm)
Lukianova et al. [59]	Four-probe method	Silicon nitride	Yttrium oxide aluminum oxide	3.16×10^{10}–1.73×10^{12}
Lukianova et al. [59]	Four-probe method	Silicon nitride	Magnesium oxide and aluminum oxide	3.87×10^{11}
Orlova [60]	Four-probe method	Silicon	Silicon carbide	3×10^{-2}– 20×10^{-2}
Soltys et al. [61]	Impedance analyzers	Glass	Alkali halide	1.09×10^{12}–2.93×10^{12}
Soltys et al. [61]	Impedance analyzers	Glass	Sodium borate	4.55×10^{3}– 6.37×10^{5}
Soltys et al. [61]	Impedance analyzers	Glass	Vanadate	4.61×10^{4}–2.13×10^{5}
Bhardwaj [5]	Four-probe method	Rice husk	Epoxy	90.9×10^{5}
Hazrol et al. [28]	Four-probe method	Sugar palm starch	Sugar palm nanocrystalline cellulose	3.14×10^{-1}–1.47×10^{5}
Devi et al. [61]	Two-probe electrode	Natural rubber	Polypyrrole	$160–1 \times 21{\cdot}10^{4}$
Naik and Mishra [62]	Concentric ring probe	Banana	High-density polyethylene	3.8×10^{14}–4.5×10^{14}
Naik and Mishra [62]	Concentric ring probe	Hemp	High-density polyethylene	3.2×10^{14}–3.8×10^{14}
Naik and Mishra [62]	Concentric ring probe	Agave	High-density polyethylene	3.3×10^{14}–3.9×10^{14}
Malik et al. [63]	Four-probe method	Silicon carbide	Boron nitride	3.7×10^{-1}–8.1×10^{-2}
Fesenko et al. [64]	Four-probe method	Aluminum nitride hexagonal boron nitride	Titanium diboride	2×10^{-3}–1×10^{-2}
Kondakov et al. [65]	Four-probe method	Titanium nitride and titanium trialuminide	Titanium aluminum nitride	3.5×10^{-4}–1.25×10^{-3}
Current studies	Four-probe method	AS	ANCC	$19{,}600 \times 10^{-3}$–$3{,}806 \times 10^{-3}$

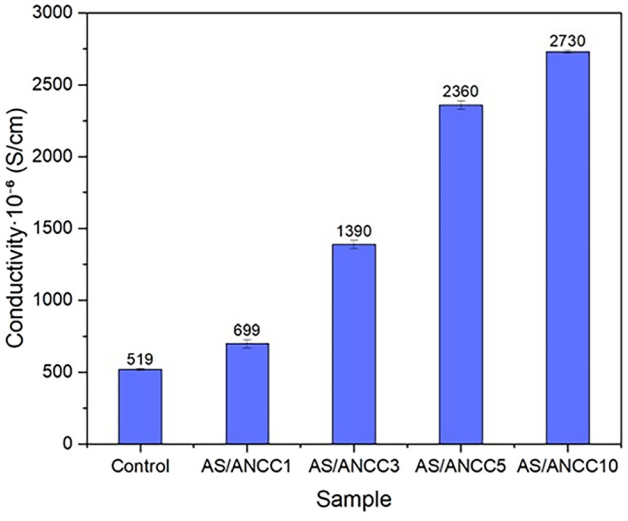

Figure 10: Conductivity of AS/ANCC biopolymer nanocomposite films.

that ANCC was an effective agent in introducing or reinforcing non centrosymmetric domains necessary in the piezoelectric activity of the starch fabric. Also, the electrical properties improved significantly besides piezoelectric performance. The pure AS films were found to be of high resistivity ($19{,}600 \times 10^{-3}$ Ω mm) that served as a good insulator. Increments in ANCC content lowered resistance to a minimum of $3{,}806 \times 10^{-3}$ Ω mm in 10 % ANCC with an increase in conductivity of 519×10^{-6} S/cm to $2{,}730 \times 10^{-6}$ S/cm. This homogenous improvement indicates that ANCC would represent as a good filler and this would facilitate the charge movement, thus raising the electrical conductivity of the biopolymer nanocomposite [71]. In general, the results show that ANCC enables the tuning of insulating biopolymer films into tunable piezoelectric and electrical films and thus broadens the potential application range in the application of such materials in sustainable electronic and sensing machines.

The promising piezoelectric and electrical properties of AS/ANCC biopolymer nanocomposites films provide significant opportunities of next generation sustainable electronic materials. To enhance the amount of interfacial polarization, even more, and the effectiveness of the charge-transport with the aid of a green coupling strategy, optimization of ANCC dispersion either with the help of surface functionalization or green coupling strategies should be considered in the future. A more in-depth mechanistic understanding of electromechanical performance would be achieved by advanced structural investigation to link crystallinity, hydrogen-bonding interactions and dipole vectors

alignment to electromechanical performance. In addition, these films will be incorporated into prototype flexible sensors, low-power energy-gathering devices, wearable biomedical patches and biodegradable electronic devices, will become necessary to confirm the relevance in real world applications. During stability tests, long-term stability tests in different humidity levels, repetitive mechanical load and environmental conditions are also needed in determining durability. Finally, full commercialisation of AS/ANCC composites into commercially viable, entirely bio-based piezoelectric systems using scale-up fabrication process with cost-effective processing methods coupled with environmentally friendly processing methods will be critical in ensuring translation of these materials into commercial smart technologies that would be environmentally friendly.

4.2 Future prospect

The future studies are to examine the underlying mechanisms that lead to these improvements, but with the specific interest in the morphology of ANCC and its interaction with the starch matrix that enhances the transport of charges. Furthermore, attempts to optimize the performance of composite at the expense of ANCC concentration and processing parameters should be made accordingly. Lastly, it will be fundamental to consider the usefulness of these materials in practice by means of creating prototypes and long-term stability, durability, biocompatibility, and biodegradability which will be the path to its successful application in the field of sustainable electronics, sensing, and biomedical purposes.

Acknowledgments: The authors wish to thank The Ministry of Higher Education Malaysia (MoHE) financed this work under the Fundamental Research Grant Scheme (FRGS), with project code of FRGS/1/2023/TK09/UPM/01/3/5540599.
Funding information: This research was supported by The Ministry of Higher Education Malaysia (MoHE) under the Fundamental Research Grant Scheme (FRGS), with project code of FRGS/1/2023/TK09/UPM/01/3/5540599.
Author contributions: All authors have accepted responsibility for the entire content of this manuscript and approved its submission.
Conflict of interest: The authors state no conflict of interest.
Data availability statement: The datasets generated and/or analysed during the current study are available from the corresponding author on reasonable request.

References

1. Uchino K. Piezoelectricity. In: Encyclopedia of RF and Microwave Engineering [Internet]; 2024:1–25. https://doi.org/10.1002/0471654507.erfme202.
2. Zhou X, Wu S, Wang X, Wang Z, Zhu Q, Sun J, et al. Review on piezoelectric actuators: materials, classifications, applications, and recent trends. Front Mech Eng [Internet] 2024;19:6.
3. Uchino K. Fundamentals of piezoelectrics. In: Olabi AGBTE of SM. Oxford: Elsevier; 2022:1–21. Available from: https://www.sciencedirect.com/science/article/pii/B9780128035818121290.
4. Balasubramaniyan C, Sampath S, Arun A, Srinivasan SA. 16 - piezoelectric devices. In: Moharana S, Sahu BB, Satpathy SK, Nguyen TABTE, EA of MO, editors. Metal Oxides [Internet]. Elsevier; 2025:423–40 pp. Available from: https://www.sciencedirect.com/science/article/pii/B978044326554900016X.
5. Ali MRR, Tigno SD, Caldona EB. Piezoelectric approaches to organic polymeric materials. Polym Int [Internet] 2024;73:176–90.
6. Liang T, Lan Y-T, Liang M-Y. Review of microstructure evolution and force-electric coupling behavior of piezoelectric materials. Mater Today Commun [Internet] 2025;47:113027. https://www.sciencedirect.com/science/article/pii/S2352492825015399.
7. Beknalkar SA, Teli AM, Satale VV, Bhat TS, Amate RU, Morankar PJ, et al. A critical review on piezoelectric supercapacitors: fundamentals, recent advances, and future directions. J Alloys Compd [Internet] 2025;1024:180169.
8. Anand A. A review on the performance enhancement techniques of piezoelectric energy harvesters. Nanomater Energy [Internet] 2025;14:62–83. https://www.sciencedirect.com/science/article/pii/S2045984X25000065.
9. Sang Y, Yang Y, Zhao Q. Electrical resistivity of plain cement-based materials based on ionic conductivity: a review of applications and conductive models. J Build Eng [Internet] 2022;46:103642.
10. Salimian F, Hemmati A, Ghaemi A. A review of nanostructured carbon dioxide sensors based on electrical and thermal conductivity. Results Eng 2025;26:105633.
11. Muhammad FAH, Sapuan SM, Mohd Afdzaluddin A, Al-Oqla FM. A review of graphene biopolymer composite in piezoelectric sensor applications; 2024;9, 12:3639–65.
12. Sapuan SM, Harussani MM, Ismail AH, Zularifin Soh NS, Mohamad Azwardi MI, Siddiqui VU. Development of nanocellulose fiber reinforced starch biopolymer composites. Review 2024;9:1171–211.
13. Ilyas RA, Sapuan SM, Norrrahim MNF, Yasim-Anuar TAT, Kadier A, Kalil MS, et al. Chapter 6 - nanocellulose/starch biopolymer nanocomposites: processing, manufacturing, and applications. In: Al-Oqla FMS Properties, and Applications of Starch and Other Bio-Based Polymers SMBTAP, editors. Elsevier; 2020. p. 65–88. Available from: https://www.sciencedirect.com/science/article/pii/B9780128196618000068.
14. Tarique J, Sapuan SM, Zainudin ES, Khalina A, Ilyas RA, Hazrati KZ, et al. A comparative review of the effects of different fibre concentrations on arrowroot fibre and other fibre-reinforced composite films. Mater Today Proc [Internet] 2023;74:411–4. https://www.sciencedirect.com/science/article/pii/S2214785322069863.
15. Firdaus AHM, Sapuan SM, Siddiqui VU, Atiqah A, Zainudin ES. Mechanical, physical and morphological properties of arrowroot starch

reinforced arrowroot nanocrystalline cellulose biopolymer nanocomposites film. Biomass Bioenergy [Internet] 2025;202:108230. https://www.sciencedirect.com/science/article/pii/S0961953425006415.
16. Jamal T, Sapuan SM, Siddiqui VU, Syamsir A. 2 - classification and properties of tuber- and root-based biocomposites. In: Sapuan SM, Abral H, Jamal T, Thakur VK, Nazrin A, et al, editors. Woodhead Publishing Series in Composites Science and Engineering [Internet]. Woodhead Publishing; 2025:11–38 pp. Available from: https://www.sciencedirect.com/science/article/pii/B9780443141263000023.
17. Tarique J, Zainudin ES, Sapuan SM, Ilyas RA, Khalina A. Physical, mechanical, and morphological performances of arrowroot (Maranta arundinacea) fiber reinforced arrowroot starch biopolymer composites. Polymers 2022;14:388.
18. Gonçalves de Oliveira Filho J, Albiero BR, Cipriano L, de Oliveira Nobre Bezerra CC, Campos Alencar Oldoni F, Buranelo EM, et al. Arrowroot starch-based films incorporated with a carnauba wax nanoemulsion, cellulose nanocrystals, and essential oils: a new functional material for food packaging applications. Cellulose 2021;28: 6499–511.
19. Tarique J, Sapuan SM, Khalina A, Sherwani SFK, Yusuf J, Ilyas RA. Recent developments in sustainable arrowroot (Maranta arundinacea Linn) starch biopolymers, fibres, biopolymer composites and their potential industrial applications: a review. J Mater Res Technol [Internet] 2021;13: 1191–219.
20. Barton RL, Keith JM, King JA. Development and modeling of electrically conductive carbon filled liquid crystal polymer composites for fuel cell bipolar plate applications. J N Mater Electrochem Syst [Internet] 2007: 225–9. https://www.scopus.com/inward/record.uri?eid=2-s2.0-37249092072&partnerID=40&md5=c17daffd8142773283da2b07ac550a02.
21. Tarique J, Salit MS, Khalina A. Extraction and characterization of a novel natural lignocellulosic (Bagasse and Husk) fibers from arrowroot (Maranta Arundinacea). J Nat Fibers [Internet] 2022;19:9914–30.
22. Ilyas RA, Sapuan SM, Ishak MR, Zainudin ES. Development and characterization of sugar palm nanocrystalline cellulose reinforced sugar palm starch bionanocomposites. Carbohydr Polym [Internet] 2018;202:186–202.
23. Boonphayak P, Muenyong N, Chinchao R, Khansumled S. Development of a biodegradable cassava starch biofilm based on a combination of plasticizers with Bio-SiO2 extracted from sugarcane leaves. Starch - Stärke [Internet] 2025;77:2300164.
24. Jomlapeeratikul P, Poomsa-Ad N, Wiset L. Effect of drying temperatures and plasticizers on the properies of konjac flour film. J Food Process Eng [Internet] 2017;40:e12443.
25. Syafiq RMO, Sapuan SM, Mohd Zuhri MYM, Othman SH, Ilyas RA. Morphological, water barrier and biodegradable properties of sugar palm nanocellulose/starch biopolymer composites incorporated with cinnamon essential oils. Phys Sci Rev 2024;9:1955–71.
26. Signore MA, Padmanabhan SK, Velardi L, Serra A, Stoppa M, Francioso L, et al. Preparation and characterization of bacterial cellulose-ZnO piezoelectric nanocomposites studied using piezoresponse force microscopy (PFM). Appl Surf Sci [Internet] 2025; 692:162734.
27. Chelly A, Glass S, Belhassen J, Karsenty A. Broad review of four-point probe correction factors: enhanced analytical model using advanced numerical and experimental cross-examination. Results Phys [Internet] 2023;48:106445. https://www.sciencedirect.com/science/article/pii/S2211379723002383.
28. Hazrol MD, Sapuan SM, Ilyas RA, Othman ML, Sherwani SFK. Electrical properties of sugar palm nanocrystalline cellulose reinforced sugar palm starch nanocomposites. Polimery [Internet] 2020;65:363–72. https://ichp.vot.pl/index.php/p/article/view/48.
29. Xu M, Wen Y, Shi Z, Xiong C, Zhu F, Yang Q. Piezoelectric biopolymers: advancements in energy harvesting and biomedical applications. Polymers 2024;16:3314.
30. Kim D, Han SA, Kim JH, Lee JH, Kim SW, Lee SW. Biomolecular piezoelectric materials: from amino acids to living tissues. Adv Mater [Internet] 2020;32:1906989.
31. Zhang S, Chen L. Theoretical model construction of piezoelectric coefficient of pbtio3 nanoparticles. Chem Eng Trans [Internet] 2017;62: 1–6. https://www.cetjournal.it/index.php/cet/article/view/CET1762001.
32. Huang G, Khan AA, Rana M, Xu C, Xu S, Saritas R, et al. Achieving ultrahigh piezoelectricity in organic–inorganic vacancy-ordered halide double perovskites for mechanical energy harvesting. ACS Energy Lett 2021;6:16–23. https://hal-univ-rennes1.archives-ouvertes.fr/hal-03124235/document.
33. Gasperini L, Selleri G, Fabiani D. Highly sensitive piezoelectric ceramic nanofibers for flexible transducers and advanced applications. IEEE 5th Int Conf Dielectrics 2024:1–4.
34. Shen ZY, Li JF. Enhancement of piezoelectric constant d_{33} in BaTiO3 ceramics due to nano-domain structure. J Ceram Soc Japan [Internet] 2010;118:940–3. https://www.jstage.jst.go.jp/article/jcersj2/118/1382/118_1382_940/_article/-char/ja/.
35. Yang L, Yang L, Cheng M, Lyu W, Shen M, Qiu J, et al. Tunable piezoelectric performance of flexible PVDF based nanocomposites from MWCNTs/graphene/MnO2 three-dimensional architectures under low poling electric fields. Compos A-Appl Sci Manuf [Internet] 2018;107:536–44.
36. Ge H, Hou Y, Zhu M, Wang H, Yan H. Facile synthesis and high d_{33} of single-crystalline KNbO3 nanocubes. ChemInform [Internet] 2009;40. https://doi.org/10.1002/chin.200906013.
37. Frick A, van Vliet WA, Žukauskaitė A, Zywitzki O, Modes T, Kostenko A, et al. Volumetric 3D-Printed piezoelectric polymer films. Adv Mater Technol [Internet] 2024;9. https://doi.org/10.1002/admt.202301469.
38. Lee M-K, Kim B-H, Lee G-J. Piezoelectric voltage constant and sensitivity enhancements through phase boundary structure control of lead-free (K,Na)NbO3-based ceramics. J Eur Ceram Soc 2022;42:4898–906. https://www.researchsquare.com/article/rs-1177124/latest.pdf.
39. Kirkpatrick M, Tarbutton JA, Le T, Lee C. Characterization of 3D printed piezoelectric sensors: determiniation of d 33 piezoelectric coefficient for 3D printed polyvinylidene fluoride sensors. IEEE Sensors [Internet] 2016:1–3. https://ieeexplore.ieee.org/document/7808876/.
40. Neugschwandtner GS, Schwödiauer R, Bauer-Gogonea S, Bauer S. Large piezoelectric effects in charged, heterogeneous fluoropolymer electrets. Appl Phys A [Internet] 2000;70:1–4.
41. Yang Y, Song C, Wang X, Zeng F, Pan F. Giant piezoelectric d_{33} coefficient in ferroelectric vanadium doped ZnO films. Appl Phys Lett [Internet] 2008;92:12907.
42. Acharya VVN, Bhanumathi A, Ramam KVS. Ferroelectric investigation of tungsten bronze lead barium lanthanum niobate ceramics with high d_{33} values. Ferroelectr, Lett Sect [Internet] 1999;25:125–8.
43. Hu Q, Alikin DO, Zelenovskiy PS, Ushakov AD, Chezganov DS, Bian J, et al. Phase distribution and corresponding piezoelectric responses in a morphotropic phase boundary Pb(Mg1/3Nb2/3)O3-PbTiO3 single crystal revealed by confocal raman spectroscopy and piezo-response

force microscopy. J Eur Ceram Soc [Internet] 2019;39:4131–8. https://www.sciencedirect.com/science/article/pii/S0955221919303656.
44. de Marzo G, Fachechi L, Antonaci V, Mastronardi VM, Portaluri L, Todaro MT, et al. On the measurement of piezoelectric d_{33} coefficient of soft thin films under weak mechanical loads: a rapid and affordable method. Mater Des [Internet] 2024;247:113399. https://www.sciencedirect.com/science/article/pii/S0264127524007743.
45. Bernard OP, Shaalan DN, Hossam M, Hassan MA. Determination of charge coefficient of piezoelectric films using a combined finite element model and dynamic loading technique. Key Eng Mater [Internet] 2020;835:229–42. https://www.scientific.net/KEM.835.229.
46. Ghosh SK, Matino F, Favrin FL, Tonazzini I, D'Orsi R, de la Ossa JG, et al. Fully biodegradable hierarchically designed high-performance nanocellulose piezo-arrays. Sci Adv [Internet] 2025;11:eads0778.
47. Mahboubizadeh S, Dilamani ST, Baghshahi S. Piezoelectricity performance and β-phase analysis of PVDF composite fibers with BaTiO3 and PZT reinforcement. Heliyon [Internet] 2024;10:e25021.
48. Liu S, Han Q, Ma N, Li C. Modulation of elastic wave propagation in piezoelectric laminated nanocomposite shells considering agglomeration effects. Acta Mech [Internet] 2022;233:5215–39.
49. Sasmal A, Maity S, Arockiarajan A, Sen S. Electroactive properties and piezo-tribo hybrid energy harvesting performances of PVDF-AlFeO3 composites: role of crystal symmetry and agglomeration of fillers. Dalt Trans [Internet] 2023;52:14837–51.
50. Han J, Kim DB, Kim JH, Kim SW, Ahn BU, Cho YS. Origin of high piezoelectricity in carbon nanotube/halide nanocrystal/P(VDF-TrFE) composite nanofibers designed for bending-energy harvesters and pressure sensors. Nano Energy [Internet] 2022;99:107421. https://www.sciencedirect.com/science/article/pii/S2211285522004992.
51. Bag N, Roy J, Mondal D, Ghosh S, Bardhan S, Roy S, et al. Utilization of experimental and theoretical piezoresponse of BTO nanocrystal for rapid decomposition of the pathogenic coliform bacteria. Ceram Int [Internet] 2024;50:7998–8009. https://www.sciencedirect.com/science/article/pii/S0272884223040488.
52. Signore MA, Francioso L, De Pascali C, Serra A, Manno D, Rescio G, et al. Improvement of the piezoelectric response of AlN thin films through the evaluation of the contact surface potential by piezoresponse force microscopy. Vacuum [Internet] 2023;218:112596. https://www.sciencedirect.com/science/article/pii/S0042207X23007935.
53. Feng CS, Zhu RK, Ming WJ, Pan K, Peng JL, Liu YY, et al. Resolving the piezoelectric properties through differential evolution algorithm via piezoresponse force microscopy. Int J Mech Sci [Internet] 2021;190:106034. https://www.sciencedirect.com/science/article/pii/S0020740320309280.
54. Zhu RK, Ming WJ, Liu YY, Pan K, Lei CH. The intrinsic piezoresponse in piezoelectric medium under contact-mode piezoresponse force microscopy. Int J Mech Sci [Internet] 2018;145:400–9. https://www.sciencedirect.com/science/article/pii/S0020740318304648.
55. Liu X, Kuang X, Xu S, Wang X. High-sensitivity piezoresponse force microscopy studies of single polyvinylidene fluoride nanofibers. Mater Lett [Internet] 2017;191:189–92. https://www.sciencedirect.com/science/article/pii/S0167577X16319498.
56. M AK, Ls J, Chandran R. Enhanced mechanical and electrical properties of styrene butadiene rubber nanocomposites with graphene platelet nano-powder. J Polym Mater [Internet] 2024;40:141–56. https://www.sciencedirect.com/science/article/pii/S0973862224000412.
57. Ilyas RA, Sapuan SM, Atikah MSN, Asyraf MRM, Ayu RS, Aisyah HA, et al. Effect of hydrolysis time on the morphological, physical, chemical, and thermal behavior of sugar palm nanocrystalline cellulose (Arenga pinnata (Wurmb.) Merr). Text Res J [Internet] 2020;91:152–67.
58. Khadka J, Ganorkar S, Lee D. Investigation of thermal emissivity and electrical resistivity of highly reflective nano-grained metal films. Appl Therm Eng [Internet] 2025;268:125854. https://www.sciencedirect.com/science/article/pii/S1359431125004454.
59. Lukianova OA, Khmara AN, Perevislov SN, Kolesnikov DA, Krasilnikov VV. Electrical resistivity of silicon nitride produced by various methods. Ceram Int [Internet] 2019;45:9497–501. https://www.sciencedirect.com/science/article/pii/S0272884218326646.
60. Orlova TS, Popov VV, Quispe Cancapa J, Hernández Maldonado D, Enrique Magarino E, Varela Feria FM, et al. Electrical properties of biomorphic SiC ceramics and SiC/Si composites fabricated from medium density fiberboard. J Eur Ceram Soc [Internet] 2011;31:1317–23.
61. Sołtys M, Górny A, Pisarska J, Pisarski WA. Electrical and optical properties of glasses and glass-ceramics. J Non-Cryst Solids [Internet] 2018;498:352–63. https://www.sciencedirect.com/science/article/pii/S0022309318301522.
62. Naik JB, Mishra S. Studies on electrical properties of natural fiber: HDPE composites. Polym Plast Technol Eng [Internet] 2005;44:687–93.
63. Malik R, Kim HM, Kim YW, Kim KJ. Grain-growth-induced high electrical conductivity in SiC–BN composites. Ceram Int [Internet] 2018;44:16394–9. https://www.sciencedirect.com/science/article/pii/S0272884218314779.
64. Fesenko IP, Kaidash OM, Sergienko N. Electrical resistivity of AlN-hBN-TiB2 ceramic composite. In: Frantsevich Ukrainian Materials Research Society; 2024.
65. Kondakov AA, Karpov AV, Grachev VV, Sytschev AE. Temperature dependence of electrical resistivity of the TiN/TiAl3/Ti2AlN composite material. Russ J Non-ferrous Met [Internet] 2020;61:216–20.
66. Ren Z, Sun J, Zeng X, Chen X, Wang Y, Tang W, et al. Research on the electrical conductivity and mechanical properties of copper slag multiphase nano-modified electrically conductive cementitious composite. Constr Build Mater [Internet] 2022;339:127650. https://www.sciencedirect.com/science/article/pii/S0950061822013253.
67. He X, Deng G, Xu H, Zhang Z, Mao H. Enhanced electrical conductivity and antibacterial properties of bacterial cellulose composite membrane decorated with hydroxypropyl-β-cyclodextrin/magnetic particle/alpha-lipoic acid/nano silver. Int J Biol Macromol [Internet] 2025;300:140281. https://www.sciencedirect.com/science/article/pii/S014181302500830X.
68. Warjri M, Narayan J. Synthesis of α-Fe2O3 nano-rod/sheet: volumetric and electrical conductivity properties of their nanofluids. J Mol Liq [Internet] 2023;377:121539. https://www.sciencedirect.com/science/article/pii/S0167732223003422.
69. Meng X, Zhang J, Ma J, Li Y, Chen Z, Liu S, et al. Using cellulose nanocrystals for graphene/hexagonal boron nitride nanosheet films towards efficient thermal management with tunable electrical conductivity. Compos A Appl Sci Manuf [Internet] 2020;138:106089. https://www.sciencedirect.com/science/article/pii/S1359835X20303286.
70. Aziz T, Rohullah UA, Ullah A, Zeb U, Hussain M, Ali A, et al. Advancements in cellulose nanocrystals: a review of functionalization, applications, and challenges. Int J Biol Macromol [Internet] 2025;315:144552.
71. Hong YJ, Roh KC, Kang YC. Superior lithium-ion storage performances of carbonaceous microspheres with high electrical conductivity and uniform distribution of Fe and TiO ultrafine nanocrystals for Li-S batteries. Carbon N Y [Internet] 2018;126:394–403.